

Article

Geology and Mineralogy of Uranium Deposits from Mount Isa, Australia: Implications for Albitite Uranium Deposit Models

Andy Wilde ^{1,*}, Alex Otto ¹, John Jory ¹, Colin MacRae ², Mark Pownceby ², Nick Wilson ² and Aaron Torpy ²

¹ Paladin Energy, Perth 6008, Australia; E-Mails: aotto@aurora-energy.ca (A.O.); john.jory@paladinenergy.com.au (J.J.)

² CSIRO Process Science and Engineering, Melbourne 3168, Australia; E-Mails: colin.macrae@csiro.au (C.M.); mark.pownceby@csiro.au (M.P.); nick.wilson@csiro.au (N.W.); aaron.torpy@csiro.au (A.T.)

* Author to whom correspondence should be addressed; E-Mail: andy.wilde@paladinenergy.com.au; Tel.: +61-8-9381-4366; Fax: +61-8-9381-4978.

Received: 1 March 2013; in revised form: 14 June 2013 / Accepted: 14 June 2013 /

Published: 26 June 2013

Abstract: New geological, bulk chemical and mineralogical (QEMSCAN and FEG-EPMA) data are presented for albitite-type uranium deposits of the Mount Isa region of Queensland, Australia. Early albitisation of interbedded metabasalt and metasilstone predated intense deformation along D₂ high strain (mylonite) zones. The early sodic alteration paragenetic stage includes albite, riebeckite, aegirine, apatite, zircon and magnetite. This paragenetic stage was overprinted by potassic microveins, containing K-feldspar, biotite, coffinite, brannerite, rare uraninite, ilmenite and rutile. An unusual U-Zr phase has also been identified which exhibits continuous solid solution with a uranium silicate possibly coffinite or nenadkevite. Calcite, epidote and sulphide veinlets represent the latest stage of mineralisation. This transition from ductile deformation and sodic alteration to vein-controlled uranium is mirrored in other examples of the deposit type. The association of uranium with F-rich minerals and a suite of high field strength elements; phosphorous and zirconium is interpreted to be indicative of a magmatic rather than metamorphic or basinal fluid source. No large intrusions of appropriate age outcrop near the deposits; but we suggest a relationship with B- and Be-rich pegmatites and quartz-tourmaline veins.

Keywords: uranium; high field strength elements; albitite-type; Valhalla; Bikini; Skal; Mount Isa; Australia; brittle-ductile transition

1. Introduction

Uranium deposits of the Mount Isa Uranium District (Queensland, Australia) are examples of the epigenetic and structurally-controlled albitite-hosted uranium deposit type, also known as metasomatite-type or Na-metasomatite-type. Albitite-type uranium deposits are widespread and economically significant but generally are poorly understood, particularly with respect to the age of ore formation, relationship to regional deformation events, the nature of the mineralising fluids, their sources and physico-chemical conditions of ore deposition [1]. Mount Isa hosts sixteen significant albitite-type resources including the world-class deposit at Valhalla and satellite deposits at Skal and Bikini (Table 1). Most of these deposits were found during the 1950s by prospectors, but with the exception of Mary Kathleen have not been developed due to low grade ($<0.1\%$ U_3O_8) and also to the perceived refractory nature of the ores.

Table 1. Uranium resources in the Mount Isa district.

Deposit	Ore (Mt)	U_3O_8 (%)	U_3O_8 (Mlbs)	U_3O_8 (t)
Valhalla	43.76	0.08	76.3	34,602
Skal	15.70	0.06	21.8	9,885
Mary Kathleen	9.20	0.12	19.6	8,891
Odin	14.00	0.06	17.6	7,964
Bikini	12.50	0.05	13.7	6,192
Anderson's Lode	1.50	0.14	5.0	2,283
Watta	5.60	0.04	5.0	2,260
Honey Pot	2.60	0.07	4.0	1,800
Mirrioola	2.00	0.06	2.5	1,132
Queen's Gift	4.40	0.02	2.4	1,080
Duke Batman	0.80	0.12	2.3	1,053
Slance	1.05	0.05	1.1	500
Citation/Mighty Glare	0.80	0.04	0.7	320
Eldorado North	0.37	0.05	0.4	170
Warawai	0.40	0.04	0.3	134
Elaine Dorothy	0.08	0.03	0.1	25
Total			172.6	78,291

Early research at the Valhalla deposit identified an ore assemblage of brannerite (containing 50% U) and an uraniferous “zircon-type” mineral (4%–8% U, 5% Zr) in a matrix which included albite, dolomite, quartz, sodic pyroxene, sodic amphibole (riebeckite) and apatite [2]. In a later study of a single drillhole from Valhalla it was proposed that the host-rocks were a sequence of metamorphosed sandstone, arkose and gritty siltstone [3]. Additional minerals identified in this later study included uraninite, calcite, chlorite, anatase and a variety of sulphides collectively defining three main

paragenetic stages [3]. Study of the Anderson's lode deposit revealed a high volume of hydrothermal fluorapatite associated with brannerite and anatase believed to predate peak metamorphism [4].

Bulk chemical enrichment of the deposits in Fe_2O_3 , Zr, Y, V and Cr has been used to relate uranium deposition to regional calcite-carbonate alteration that is particularly well developed along north-south trending structures (Figure 1) [5,6]. Additionally, enrichment in Na, Ca, P, Sr and F with depletion in K, Ba and Si has been noted at Valhalla [3]. Ar-Ar and U-Pb isotopic dates have been obtained from three of the deposits [3,7,8] and stable isotope data obtained from Valhalla [3]. Many of the deposits listed in Table 1, however, have not been previously described.

Despite these studies there is a lack of consensus on the origin of these unusual deposits. Involvement of basinal brines has been proposed by several authors [3,5,6]. Stable isotope data are consistent with this interpretation but also with a magmatic fluid origin [3]. Conversely, the inferred temporal relationship between uranium and peak metamorphic features at Anderson's Lode has been used to argue the deposits represent metamorphosed unconformity types [4]. Recently, it has been proposed that the unusual chemical signature of the deposits is inconsistent with isochemical metamorphism of unconformity-type deposits but instead that the deposits are derived from granitic intrusions [9].

In this study we present new data on the geology, bulk chemistry and mineralogy of the Mount Isa district uranium deposits, chiefly Valhalla, Bikini and Skal, based on resource drilling campaigns between 2008 and 2011 and surface mapping of the Bikini and Skal deposits. We present new mineralogical observations based on examination of over 100 thin sections including samples from nine other deposits. Sixty-six thin sections have been examined by quantitative scanning electron microscopy (QEMSCAN) and high resolution electron microprobe. These new data reveal previously unrecognised complexity of the deposits with variation in ore and gangue mineralogy apparent at thin section, deposit and regional scales. The relationship of the various paragenetic phases to recognised deformation events is clarified and some new insights into the processes of ore genesis are presented.

2. Geology of the Mount Isa Uranium District

The Mount Isa uranium district is located within a major Proterozoic terrane that is well-endowed with world-class base-metal deposits (Mount Isa Cu, Mount Isa, George Fisher and Hilton Pb-Zn) as well as the uranium deposits that are the subject of this paper (Figure 1). Nearly all the uranium deposits of the Mount Isa uranium district are hosted by the Eastern Creek Volcanics (ECV) a 7 km thick sequence of extrusive metabasalt layers up to 100 m thick with interbedded metasediments (Figure 1) [6]. Re-Os dating of weakly metamorphosed ECV metabasalt returned an isochron of 1.83 ± 0.05 Ga, probably the best estimate of extrusion age [10]. Rocks of the ECV are intruded by the Sybella batholith dated by U-Pb zircon at 1657 ± 7 Ma [11]. The Kitty Plains microgranite, which forms the north-eastern part of the Sybella batholith is radiometrically anomalous and has been cited as a possible source of uranium [9]. Recent dating of this intrusion using the U-Pb zircon technique has yielded an age of 1670 ± 9 Ma with a later disturbance at 1589 ± 29 Ma [9].

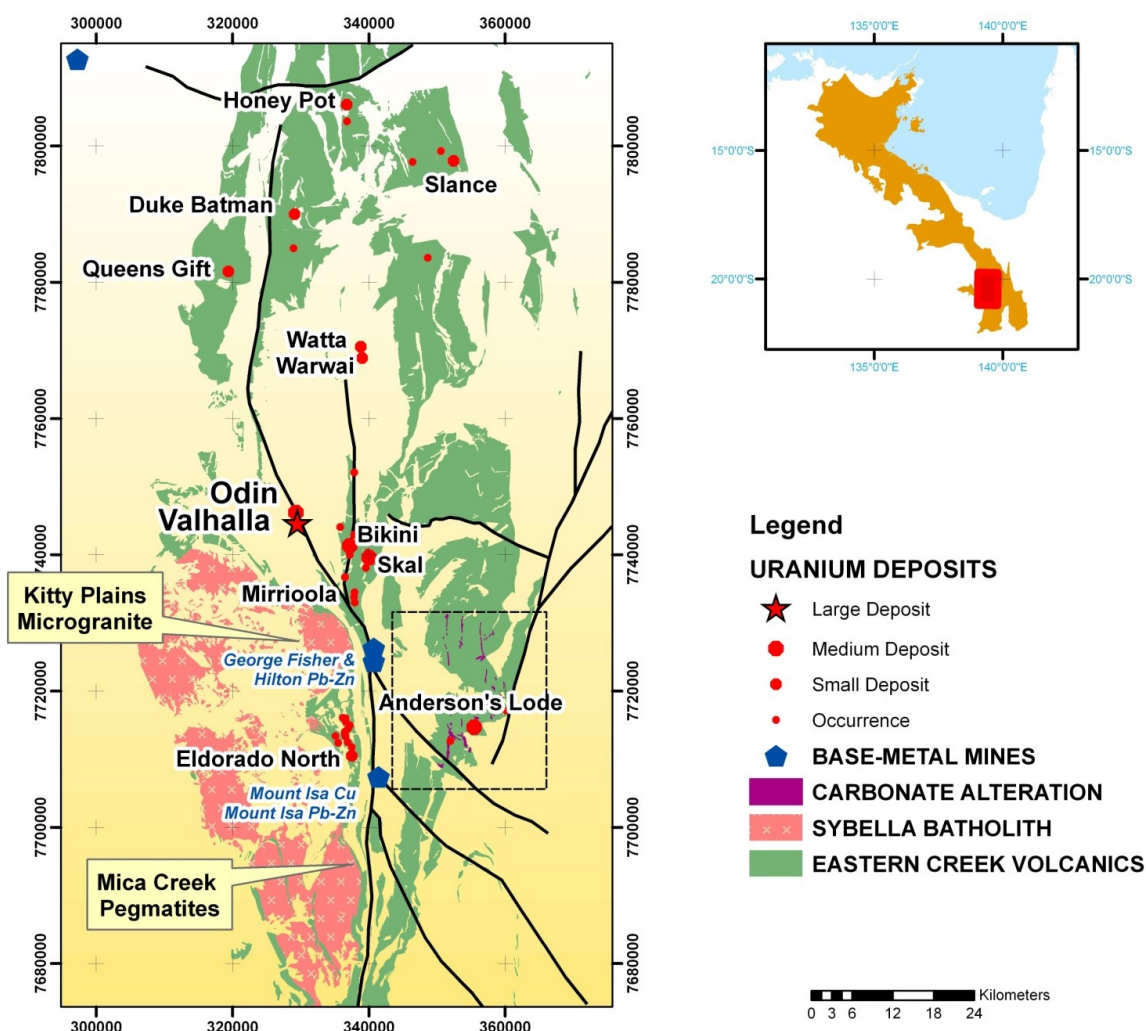
The architecture of the Mount Isa area is to a large degree a product of east-west compression during the Isan orogeny (D_2). This deformation has imposed a north-south grain (Figure 1). Rocks of the ECV dip steeply, but it is rare to observe fold closures in the field, except in high strain zones that

host uranium deposits, and individual sedimentary interlayers can be traced with remarkable continuity over considerable distances. Regional metamorphism accompanying the Isan orogeny reached greenschist facies over much of the uranium district, but reached amphibolite facies and higher adjacent to the Sybella batholith [12]. The absolute age of the peak of regional D₂ metamorphism and deformation has been established at 1591 ± 10 Ma by dating monazite encapsulated in syn-D₂ garnet, staurolite and andalusite [13].

Pegmatites are abundant in the Mica Creek area contain quartz, microcline, albite, muscovite and tourmaline with accessory beryl, apatite, garnet and locally monazite [11]. An attempt to date various generations of these pegmatites using the U-Pb zircon technique obtained ages of 1565 ± 5, 1532 ± 7 and 1480 ± 14 Ma, but failed to recognise the metamict nature of the dated zircons [11].

Later ductile events are recognised but have had little impact on the gross architecture of the district. Of particular significance to uranium deposits are NW-SE-trending shear zones defined by chlorite schist (Figure 1). The latter structures cut and displace uranium deposits and are implicated in sediment-hosted copper formation at Mount Isa [14].

Figure 1. Simplified geology of part of the Mount Isa uranium district. The location map shows the extent of the North Australian Proterozoic province in orange. The dashed rectangle shows the extent of 1:35,000 scale mapping of regional carbonate-iron oxide alteration [6].



Regional hydrothermal alteration within rocks of the ECV in the vicinity of Mount Isa has been extensively documented, mostly in the context of tracing flow paths for oxidised brines that formed the Mount Isa copper deposits [5–7,12,15–17]. Of most relevance to this study are albite (\pm tremolite), carbonate-iron oxide and tourmaline types. Carbonate (mainly calcite) and iron oxide alteration has been mapped in the Haslingdon area where it is associated with NS trending structures (Figure 1) [6]. Calcite postdates the main compressional deformation (D_2) since carbonate veins overprint the regional S_2 cleavage [6]. Locally, intense hematite alteration within these carbonate-rich zones is associated with elevated gamma radiation [6].

Boron metasomatism is quite extensive in several areas south-west of Mount Isa including the Mica Creek area (Figure 1) and is spatially associated with several uranium deposits [15]. Locally, boron metasomatism has produced near massive tourmaline rocks, typically adjacent to Syn- D_2 quartz-tourmaline veins [15]. Quartz-tourmaline veins adjacent to the Eldorado North and Anderson's Lode uranium deposits have been dated at 1577 ± 48 and 1573 ± 12 Ma suggesting that substantial boron metasomatism occurred during or soon after peak metamorphism [15].

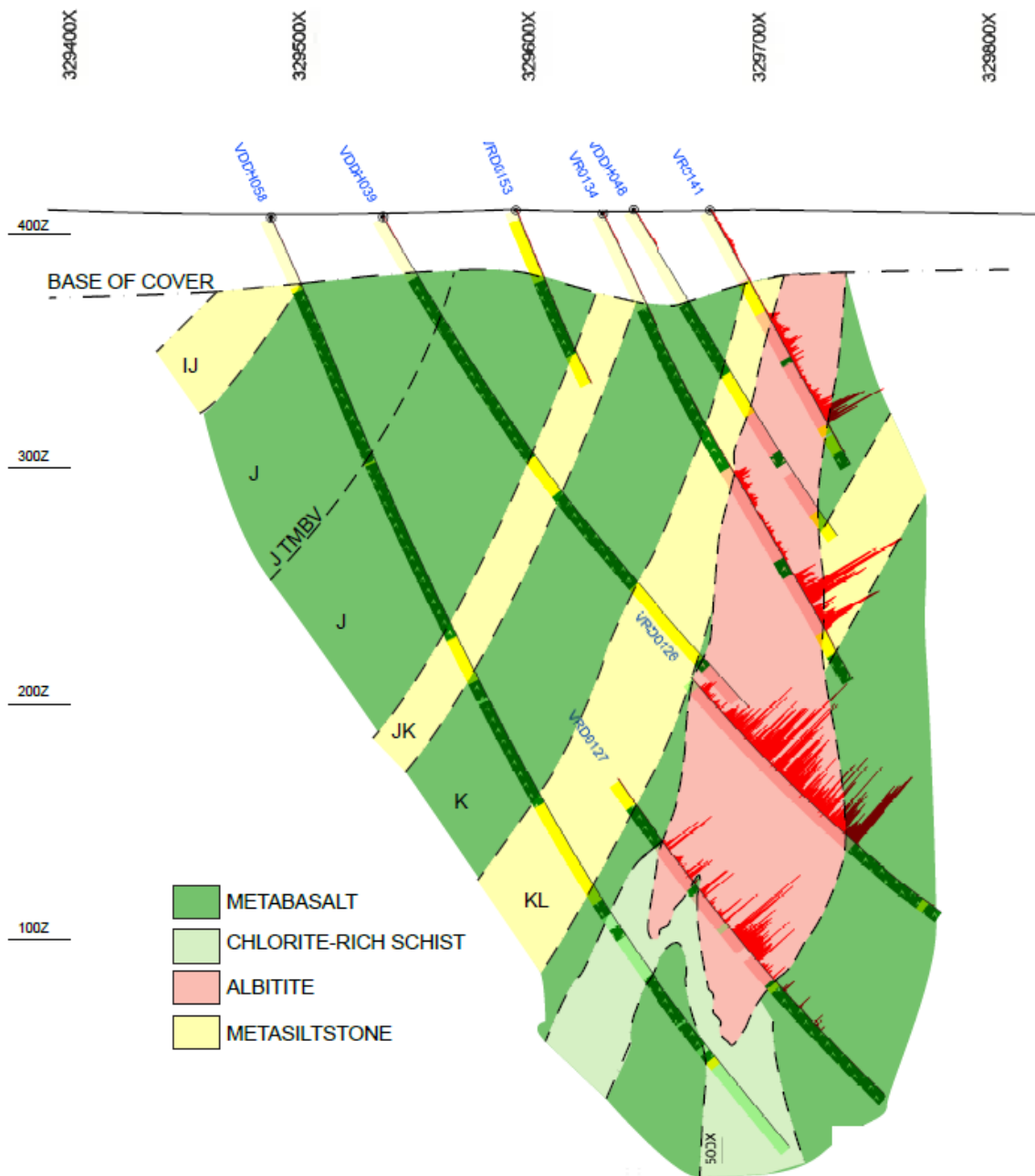
Albitite within the area of Figure 1 is rare. Most known occurrences of albitite are associated with uranium mineralisation. The exceptions are albite-tremolite rocks to the west of Mount Isa [12] and albitic meta-siltstones (Spear-Kennedy Siltstone) at the Mount Isa copper mine. The latter have not been studied in any detail, but appear to be peripheral to an hydrothermal anhydrite-dolomite-hematite body [14]. Albite-tremolite rocks form small (<35 m) bedding-parallel pods associated with north-south trending quartz veins. Tremolite is in some cases aligned parallel to S_2 , but in others forms randomly oriented sprays, leading to the conclusion the albite-tremolite pods formed "late to post- S_2 " [12].

3. Geology of the Deposits

The Valhalla deposit is completely buried by younger cover and knowledge of its geology comes from over 600 drillholes. Figure 2 shows a typical cross-section, illustrating a near-vertical body of albitite and minor chlorite schist that varies in width from 50 to 75 m. Interlayered metabasalt and meta-sediment comprise the western (hanging wall) side of the albitite body. The bulk of the hanging wall sequence in these sections is made of two thick metabasalt units, termed J and K, with three metasedimentary layers termed IJ, JK and KL. Metabasalt unit J is the thickest in the deposit (approximately 100 m). A thin marker of metasiltstone (J_{tmb}) occurs in the middle of this unit. A slight angular discordance between the metabasalts and metasiltstones and the albitite body is apparent (Figure 2). Displacement of the metasiltstone layers is also apparent but it is difficult to correlate individual layers across the albitite body with confidence, and thus the sense of movement is uncertain. Measurements of the main S_2 foliation in oriented core show that S_2 trends parallel to the trend of the main albitite body.

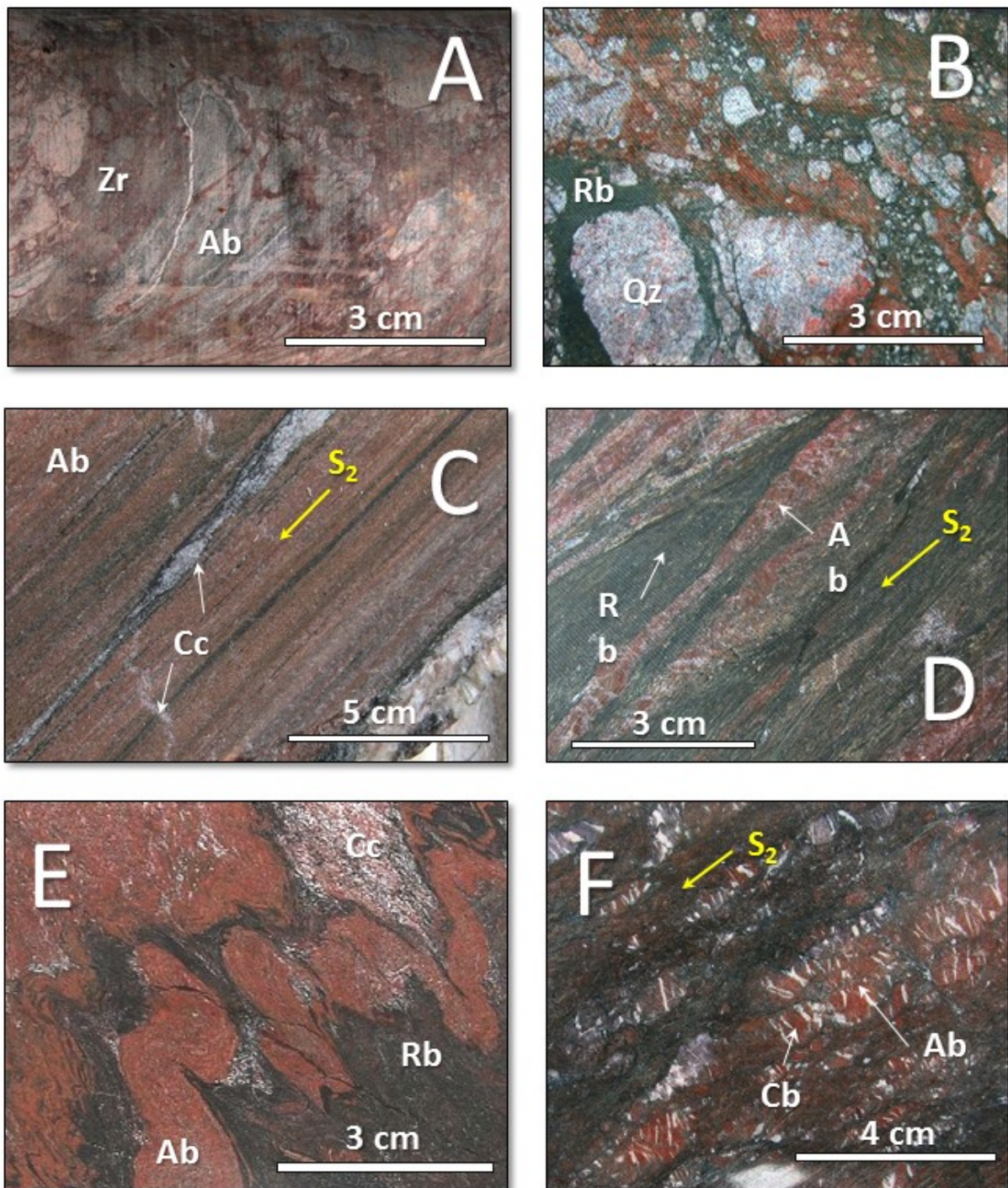
Uranium is hosted within the north-south striking transgressive albitite and to a much lesser extent in peripheral chlorite-rich schist. The intersection of bedding and albitite appears to be an important control on ore distribution as evidenced by higher grade uranium ore plunging parallel to the intersection lineation of bedding and the albitite body. This interpretation is consistent with inferred controls on uranium distribution in the Haslingdon area [6].

Figure 2. Cross-section 7744850 mN, Valhalla deposit. The red bars on drillhole traces represent the tenor of uranium mineralisation.



The albitites are pink to salmon-red to dark green rocks that are the altered equivalents of metabasalt and metasediment. The albitites have three textural variants: massive, laminated and brecciated (Figure 3). Massive albitite at Valhalla accounts for approximately 20% of the total ore and laminated and breccia type 40% each. The laminated type is texturally similar to a mylonite. This ore type has previously been termed “LIAR” or laminated and intensely altered rock [3]. Breccia ore contains the best uranium grades and has previously been termed “BIAR” or brecciated and intensely altered rock (Figure 3A) [3]. A fourth ore type, consisting of uraninite, hematite, dolomite and chlorite (UHDC) veins has been described from drillhole V39 (renamed to VDDH039—Figure 2) where it locally comprises as much 5% of the ore [3]. This ore type appears to be rather rare in the rest of the orebody.

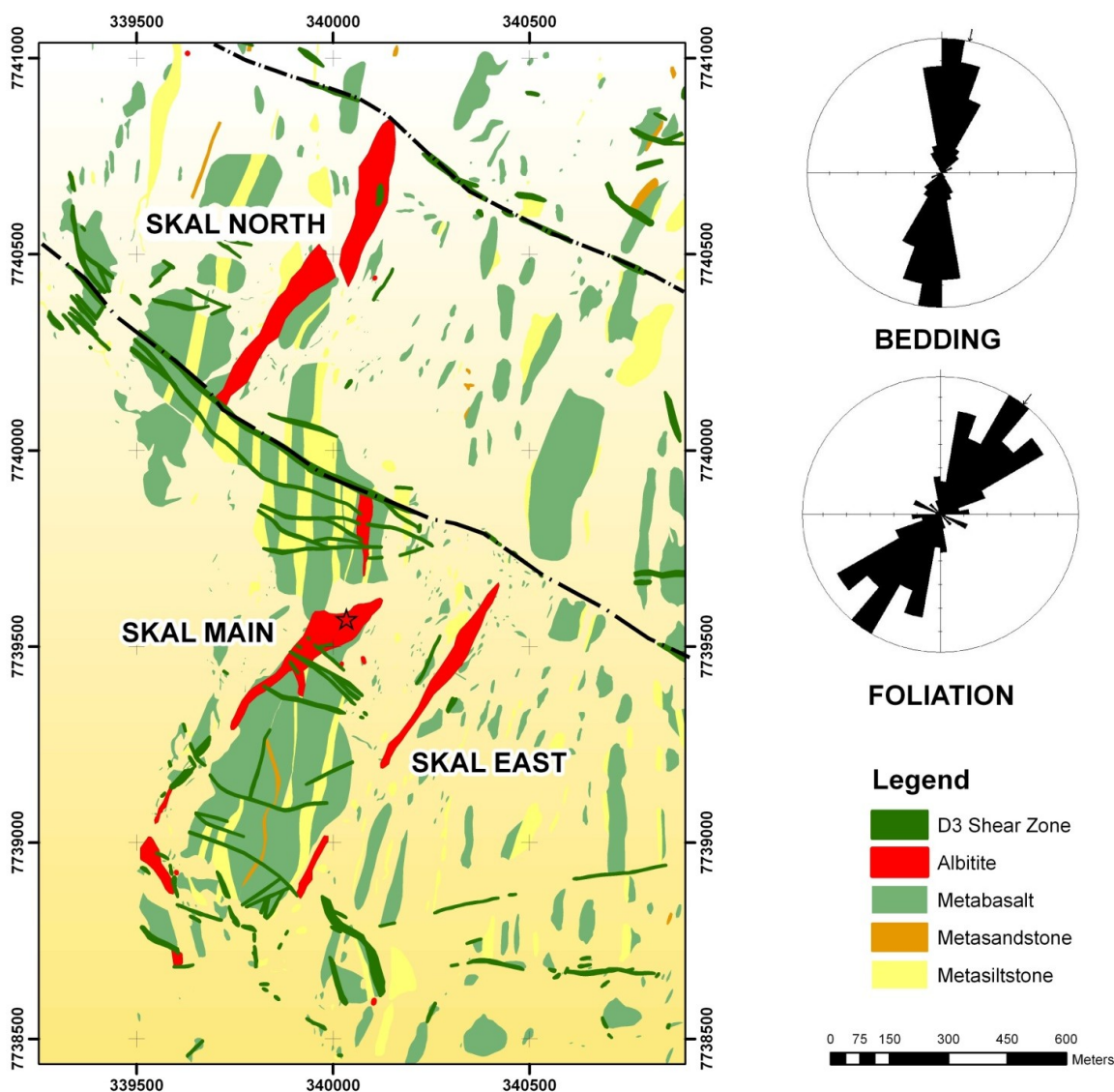
Figure 3. Examples of rock types from the Mount Isa uranium region: (A) Valhalla VRD185 232.1 m. Brecciated albitite (Ab) with matrix of dark red hydrothermal zircon (Zr). (B) Skal SD084 56.4 m. Breccia of rounded early quartz vein fragments in dark green riebeckite-rich matrix. (C) Typical laminated ore, Bikini BPDD024 169 m. Ab, Albitite. Cc, late calcite vein emplaced parallel to and transgressive to S_2 . (D) Bikini BPDH051 92 m. Boudinaged lithons of albitite (Ab) enveloped by spaced S_2 domains defined mainly by riebeckite (Rb). Cc, calcite-rich area. (E) Mirrioola MIDDH012 109 m. Folded albitite (Ab) with partially transposed limbs. Riebeckite-rich matrix (Rb). (F) Queen’s Gift QGDC008 81.5 m. Similar to (E), showing greater abundance of milky white carbonate (Cb) veinlets.



In contrast to Valhalla, there is substantial outcrop at Skál. Figure 4 illustrates the north-south strike of bedding which dips consistently at 80° NW and the slightly discordant disposition of several steeply-dipping albitite bodies. Foliation is well developed at Skál. The main S₂ foliation is a spaced cleavage which is associated with a substantial component of transposition [18,19]. S₂ in mineralised drillcore is defined by planar or anastomosing riebeckite-rich zones, often wrapping around albite-rich lithons. Folded or boudinaged albitic lithons are frequently observed to be cut by perpendicular carbonate-rich veinlets which terminate at the contact between the albite-rich lithon and enveloping riebeckite-rich S₂ [18,19]. A feature of the Skál deposits is the presence of early quartz veins which have been dismembered and included in breccias such as that illustrated in Figure 3B.

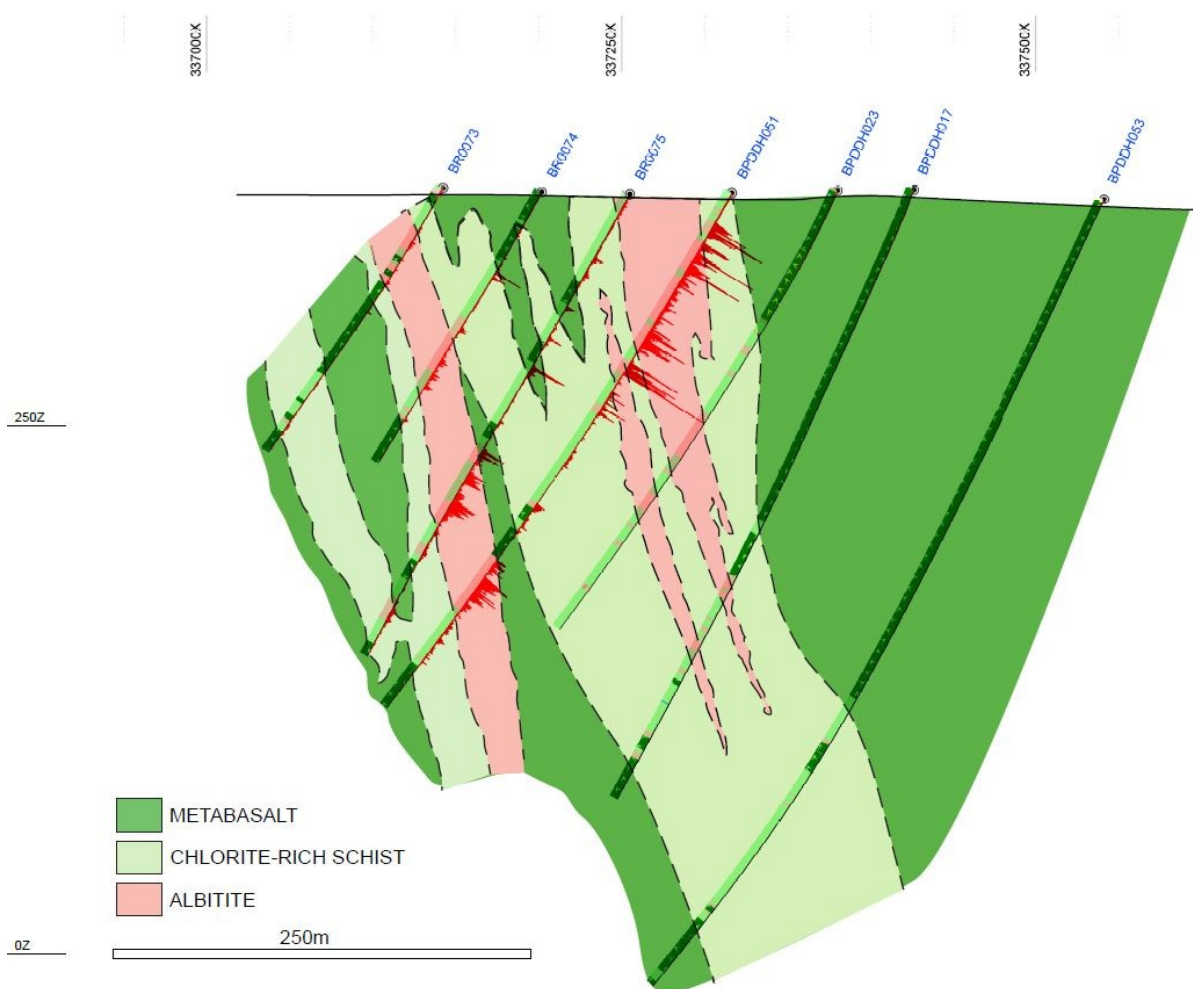
Late, anastomosing shear zones trending north-west to south-east are clearly visible. The main Skál albitite body is inferred to have been dismembered and offset by approximately 1 km by one such 250 m wide deformation zone. A late set of spaced cleavage, S₃, may be related to this event and is defined by seams and fracture fill of chlorite and calcite overprinting S₂ [19]. Late kinks have also been identified [19].

Figure 4. Outcrop map of the Skál deposit. The foliation is the dominant S₂ fabric.



Mapping at Bikini clearly shows that uranium is associated with a high strain zone which is very similar to those hosting the Skål and Valhalla deposits [18–20]. There are two substantial differences, however. One is that the albitite forms several discrete layers, rather than a single mass. There is also a much higher volume of quartz-chlorite schist, although this lithology hosts a relatively small portion of the uranium resource (Figure 5). Bedding at Bikini strikes overall at 055° and dips at 87° NE, while the main foliation, again S_2 , is slightly discordant striking at 027° and dipping nearly vertically [19]. The intersection of bedding and the main S_2 foliation therefore plunges nearly vertically. Albitite is typically parallel to the S_2 foliation and discordant to bedding, probably the result of folding and transposition during D_2 (Figure 3C,D) [18–20]. Several rootless fold closures have been identified at outcrop within the highly strained and albitised metabasalt [18–20] and it is possible that individual layers as shown in Figure 5 represent limbs of a tight fold or folds.

Figure 5. Representative NW-SE cross-section of the Bikini deposit.



Duke Batman is significantly different to Valhalla, Skål or Bikini [21]. Albitite is volumetrically much less common at Duke Batman while biotite and potassium feldspar are correspondingly more abundant. It is also distinguished by the fact that the host high strain zone is oriented more east-west than north-south. Structural studies have yet to be undertaken at Duke Batman. Anderson's Lode differs from the other deposits in being hosted predominantly within metasandstone and metaconglomerate, and has a high concentration of hydrothermal apatite.

4. Bulk Chemistry and Mineralogy

4.1. Methods

Bulk geochemical data for 90 samples of the Valhalla deposit were obtained to examine bulk chemical characteristics of ore, altered rocks and protolith. Analysis was by ICP-MS following four acid digest, and conducted at a commercial laboratory.

QEMSCAN is an abbreviation of quantitative evaluation of minerals by scanning electron microscopy, and comprises a scanning electron microscope, up to four light-element energy-dispersive X-ray detectors and proprietary software. The technique creates mineral maps of a thin section surface by scanning with an high-energy accelerating electron beam along a predefined raster scan pattern, and permits determination of mineral grain size and shape, mineral associations, mineral liberation, elemental deportment and porosity. Another useful function is the determination of relative volumes of minerals. Sixty-six samples were sent to two commercial laboratories for analysis [22–24].

Five thin sections were subjected to electron microprobe microanalysis (EPMA) using a JEOL 8500 FEG-EPMA (Tokyo, Japan) at CSIRO's Clayton Microbeam Laboratory, particularly to take advantage of its superior spatial resolution and analytical capabilities. Uranium-rich regions were mapped using wavelength dispersive (WDS; Al, Si, U, Pb and S) and energy dispersive (EDS) spectroscopic techniques. Standards included spinel ($MgAl_2O_4$), wollastonite ($CaSiO_3$), uraninite (UO_2), anglesite ($PbSO_4$), pyrite (FeS_2), spinel ($MgAl_2O_4$), baddeleyite (ZrO_2), hafnium metal (Hf), yttrium vanadate (YVO_4), hematite (Fe_2O_3) and cerium oxide (CeO_2). Operating conditions for mineral mapping were accelerating voltage 12 kV, beam current 60 nA, step size 400 nm and 40 ms. per step counting time. Operating conditions for quantitative mineral analysis were 15 kV, and 5 nA, and the beam was defocused to between 5 and 10 μm to minimise migration of elements under the beam. A *phi-rho-Z* matrix correction based on the CITZAF routine [25] was employed for correct for absorption, fluorescence and atomic number effects. Element distribution data were manipulated using the software package Chimage [26].

4.2. Valhalla

Unaltered metabasalts at Valhalla are typically dark green, fine-grained and textureless in core samples, although vesicles are locally preserved and vesicle-rich zones define the tops of individual meta-basalt layers. Under the microscope, metabasalts commonly preserve igneous texture with lathes of albitic plagioclase (pseudomorphing magmatic feldspar) in a ground mass of chlorite with minor epidote, biotite, calcite, magnetite and ilmenite. The metasiltstone protolith is dominated by quartz, muscovite and biotite with accessory (formerly detrital) magnetite, hematite and ilmenite [3]. While most metasediments appear to be derived from siltstones, cross-bedded sandstones and conglomerates are also present [3].

Table 2 and Figure 6 illustrate differences in bulk chemical composition between Valhalla protolith lithologies (metabasalt, metasediment) and altered equivalents (albitite and chlorite schist). Albitisation has resulted unsurprisingly in bulk gain in Na_2O . Albitite contains an average 6.64% compared to protolith averages of 2.53% (metabasalt) and 1.75% (metasediment). Table 2 also reveals

dramatic loss in K relative to both protolith types, confirming an earlier observation [3]. Furthermore, SiO₂ depletion is extreme relative to metasediment, but less so with respect to the metabasalt protolith.

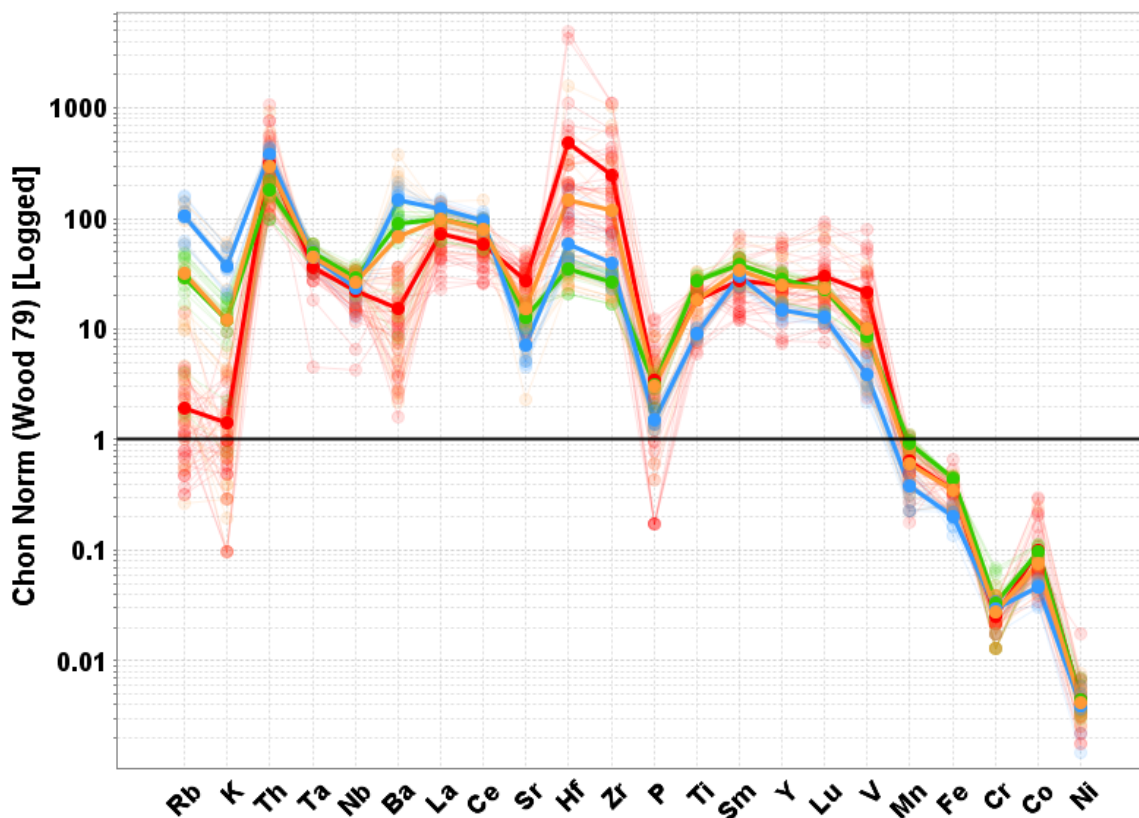
Table 2. Bulk chemical analyses of various rock types from Valhalla.

Oxide/Element	Meta-Basalt			Meta-Sediment			Chlorite-Carbonate Schist			Albitite		
	n = 16			n = 12			n = 21			n = 41		
%	Mean	Min	Max	Mean	Min	Max	Mean	Min	Max	Mean	Min	Max
SiO ₂	49.1	48.7	49.7	58.3	54.4	62.7	48.1	39.3	58.3	47.4	39.6	56.8
TiO ₂	2.75	2.05	3.21	0.92	0.81	1.05	1.98	0.77	3.38	1.79	0.61	2.74
Al ₂ O ₃	12.6	11.9	13.5	13.7	9.1	18.0	13.6	10.2	17.5	10.3	5.4	14.5
Fe ₂ O ₃	16.8	15.2	17.7	7.7	5.2	10.2	13.3	8.0	18.4	13.0	7.8	20.2
MgO	4.39	3.54	5.62	2.86	1.75	3.25	3.86	3.18	5.16	3.87	2.34	6.69
MnO	0.20	0.16	0.25	0.08	0.05	0.14	0.14	0.06	0.25	0.14	0.05	0.24
CaO	7.58	5.62	8.51	5.06	1.64	10.90	6.38	1.38	11.65	7.15	3.22	11.95
K ₂ O	1.23	0.08	1.93	3.75	2.05	5.65	1.70	0.07	6.15	0.13	0.01	0.96
Na ₂ O	2.53	1.34	4.33	1.75	1.24	2.80	3.80	0.30	6.13	6.64	3.71	8.71
P ₂ O ₅	0.35	0.22	0.47	0.17	0.14	0.23	0.31	0.14	0.57	0.39	0.02	1.40
LOI	2.08	1.54	2.79	5.54	3.40	9.84	6.55	3.00	11.58	8.29	2.93	12.44
Total	99.76	99.59	99.97	99.92	99.72	100.05	99.79	99.51	100.05	99.01	94.26	99.99
ppm												
Nb	15.5	10.7	21.4	13.1	7.2	15.9	14.6	9.6	19.9	13.0	3.7	20.0
Ta	1.0	0.7	1.3	0.9	0.7	1.2	1.0	0.7	1.3			
Zr	231	138	304	354	205	1,030	237	162	432	2,411	265	>10,000
Hf	6.3	3.7	9.2	11.2	6.5	34.8	6.6	4.4	9.2	90.2	6.6	921.0
Y	51.9	32.1	68.3	29.4	23.1	35.1	44.1	26.9	63.1	51.6	14.8	132.0
Th	6.9	3.6	9.6	15.3	10.9	18.0	10.5	6.1	17.2	12.9	3.8	42.8
U	2.0	1.0	2.6	12.5	4.1	59.6	10.6	2.0	50.5	387.3	15.1	>1,000
V	401	288	499	188	107	286	305	133	507	979	117	2780
Cr	84	30	160	68	40	80	67	30	110	55	30	80
Co	45.4	35.8	53.3	21.5	14.2	25.9	33.3	18.5	51.4	43.2	16	134.5
Ni	45	28	68	36	14	56	39	26	56	41	17	168
Cu	193	57	385	47	5	260	85	6	281	812	25	7110
Zn	148	91	176	86	59	101	104	50	162	66	25	140
Pb	7	<5	14	10	<5	17	10	<5	19	124	<5	657
Ga	22.8	18.5	25.9	20.9	13.8	27.3	22.4	13.6	28.4	16.2	12.1	24.8
Rb	50.7	3.1	92.1	200	106	300	79.9	1.1	269	4.7	0.5	52.8
Cs	2.51	0.21	6.05	4.88	2.65	7.8	2.27	0.11	6.73	0.29	0.01	4.19
Sr	134	105	185	76	47	127	133	24	238	275	55	525
Ba	303	30.4	536	535	290	762	320	7.9	1355	55.6	5.8	262
La	30.6	18	39.7	40	32	49.9	34.3	25	46.7	24.1	7.6	46.6
Ce	67.5	41.1	87	82.1	66.7	101	71.6	53.8	83.8	52.7	22	128.5
Pr	7.4	4.65	9.5	8.41	6.65	10.4	7.64	5.68	8.87	5.8	2.32	14.35
Nd	30.8	19.4	40.3	31.7	25.3	39	30.7	22.4	38	24.3	9.9	59.3
Sm	7.36	4.73	9.61	6.17	4.83	7.64	6.77	5	8.75	5.84	2.45	14.3
Eu	2.04	1.45	2.48	1.19	0.91	1.46	1.64	1.08	2.46	1.57	0.49	4.82
Gd	8.25	5.34	10.5	5.73	4.66	6.8	7.32	4.89	10.3	6.64	2.53	17.35

Table 2. Cont.

Oxide/Element	Meta-Basalt n = 16			Meta-Sediment n = 12			Chlorite-Carbonate Schist n = 21			Albitite n = 41		
	Mean	Min	Max	Mean	Min	Max	Mean	Min	Max	Mean	Min	Max
Tb	1.54	0.94	1.97	0.93	0.73	1.11	1.31	0.83	1.9	1.29	0.4	3.67
Dy	8.41	5.24	10.8	4.97	3.79	5.9	7.2	4.38	10.45	7.72	2.13	20.7
Ho	1.86	1.18	2.38	1.02	0.78	1.18	1.56	0.97	2.29	1.78	0.49	4.6
Er	5.13	3.18	6.66	3.01	2.38	3.42	4.36	2.72	6.36	5.59	1.61	14.65
Tm	0.76	0.47	1.21	0.46	0.35	0.54	0.65	0.43	0.93	0.93	0.26	2.54
Yb	5.04	3.09	6.67	2.9	2.36	3.45	4.34	2.83	6.14	6.82	1.87	19.45
Lu	0.72	0.44	0.93	0.43	0.39	0.51	0.62	0.39	0.87	1.03	0.26	3.19
Density	3.05	2.91	3.16	2.79	2.67	2.89	2.87	2.71	3.05	2.89	2.29	3.12

Figure 6. Chondrite-normalised spidergram of selected elements in Valhalla albitites (plotted using the method of [27]). Solid lines represent average compositions for the four rocktypes in Table 2. Red, albitite; orange, chlorite and riebeckite schist; green, metabasalt; blue, metasilstone.



Trace element data show that the albitite is enriched in zirconium (average 0.24%), hafnium (average 90 ppm, mainly located in zircon), copper (average 812 ppm as chalcopyrite) and vanadium (average 979 ppm) relative to either protolith lithology. Uranium in the albitite and schist samples correlates well with a range of high field strength elements (HFSE) including Zr, Hf, HREE and Th (Pearson coefficients generally >0.7), but excluding LREE (La, Sm, Nd) and Ta.

Nineteen mineralised samples from Valhalla were quantified using QEMSCAN. Four uranium minerals were found: coffinite, uraninite, brannerite and an unidentified U-Zr phase consistent with previous observations [2,3]. Brannerite, however, was noted in only three samples, and in only one sample is it abundant relative to other uranium phases. A uraniferous zirconium-rich phase occurs in about half of the samples from Valhalla, varying from 5% to 33% of uranium-bearing phases but accounting for less than 5% of contained uranium as the uranium content is usually <10%.

Clearly uranium minerals vary substantially in type and abundance between samples, and this is suggestive of variation at the deposit scale. This may explain why the first published work on Valhalla mineralogy failed to mention uraninite or coffinite [2] and emphasises the need to examine as representative collection of samples as possible.

Albite and amphibole comprise 54% of the Valhalla samples. Carbonate minerals (calcite, dolomite and ankerite) comprise a further 8.9%. The average abundance of hydrothermal apatite and zircon is striking, at 7.8% and 5.6%, respectively. Zircon (*sensu stricto*) was found to exceed 10% in three samples reaching a maximum of 25%. Apatite exceeded 10% in 6 samples and reached a maximum of 27%. Chlorite makes up a relatively small volume of the samples with an average content of 4.1%. Aegirine has been identified by hyperprobe, confirming an early study [2].

Mineral mapping using hyperprobe and QEMSCAN reveals many significant textural and paragenetic features. Albite-rich domains are typified by the images in Figures 7 and 8, in which albite exhibits interlocking “chicken-wire” texture and apparently coexists with fluorapatite and riebeckite. Previous SEM study of these amphiboles has documented variation from cores rich in Na and Fe to rims rich in Mg and Ca (*i.e.*, from riebeckite to more hornblendic compositions [3]). Albite encloses a large number of subhedral inclusions of (low uranium) zircon which are shown as Zr silicate (U, Ca, Al) in Figure 7. Figure 8 illustrates the association of albite with coarse euhedral magnetite. This albite-zircon-apatite-amphibole-magnetite assemblage is interpreted to represent the earliest hydrothermal stage at Valhalla. This differs from previous work [3] by including hydrothermal apatite and zircon with this early sodic alteration stage.

Figure 8 illustrates a later overprint of several types of veinlet on the early albitite assemblage. We interpret the textures in Figure 8 to indicate that albite-rich domains are cut by veins and patches of dolomite. Dolomite, in turn, is cut by and enclosed within quartz. Calcite can be seen to occupy a late fracture and what appears to be vuggy cavity in dolomite, and as angular grains enclosed in quartz.

In many samples coffinite is spatially related to riebeckite, but in several cases was observed to occur in veinlets that cross-cut and enclose fragments of riebeckite. Another mode of occurrence is as veinlets that exploit grain boundaries between albite grains. Coffinite veinlets were also observed to cut relict detrital magnetite and quartz. An unusual occurrence is as inclusions in albite, but their shape suggests that coffinite replaced former riebeckite inclusions. Coffinite veinlets tend to be monominerallic but sometimes are associated with chlorite, rutile and K-feldspar. Coffinite veinlets and patches are clearly cut and therefore postdated by calcite-epidote veinlets.

Analyses of discrete grains of uranium silicate by FEG-EPMA returned an uranium content of 58 wt %, well below the stoichiometric value of 80 wt % U for coffinite and totals averaging 92%, confirming data from a previous study [3]. It has been proposed that the Valhalla coffinite may be metamict or amorphous [3,28]. An alternative is that the uranium silicate with low analytical totals is nenadkevite, an hydrated uranium silicate containing both U⁴⁺ and U⁶⁺ [29] rather than coffinite.

Brannerite was almost always found to be associated with composite K-feldspar-quartz-ilmenite-rutile veinlets as shown in Figure 8. Such veinlets unequivocally cut the albite-dolomite assemblage. Quartz is apparently cut by a K-feldspar-brannerite veinlet in Figure 8.

A uraniferous zirconium mineral (Zr silicate (U, Ca, Al)) has been observed as ultra-fine veinlets along albite grain boundaries often emanating from occurrences of rounded U-poor zircon (Figures 7 and 9). It is significantly more uranium-rich than the more rounded grains included in albite and grades laterally into coffinite (Figure 9). This mineral was found to be extremely sensitive to the electron beam, and very low beam currents together with short count times were required to correctly measure elemental concentrations. The uranium content of this phase averages 32% but ranges from 17% to 53%, Zr ranges from 25% to 1% and totals average 85%. There appears to be a correlation between the uranium content of the U-Zr phase and proximity to coffinite-rich regions, being most uranium-rich when coffinite is close by. The range of composition of this U-Zr phase is consistent with a solid solution between hydrated equivalents of $USiO_4$ (possibly nenadkevite) and $ZrSiO_4$ (Figure 10). The U-Zr phase is depleted in Zr, Hf and Si and enriched in U, Al, Fe and Ca relative to zircons related to the early sodic alteration assemblage.

Uraninite was not present in the samples analysed by us using FEG-EPMA, but analyses have been previously reported and show anomalously low Pb contents attributed to post-depositional alteration of uraninite (calculated “chemical” ages varied from 9 to 165 Ma) [3].

Figure 7. Phase patched map of sample from Valhalla drillhole VRD0205.

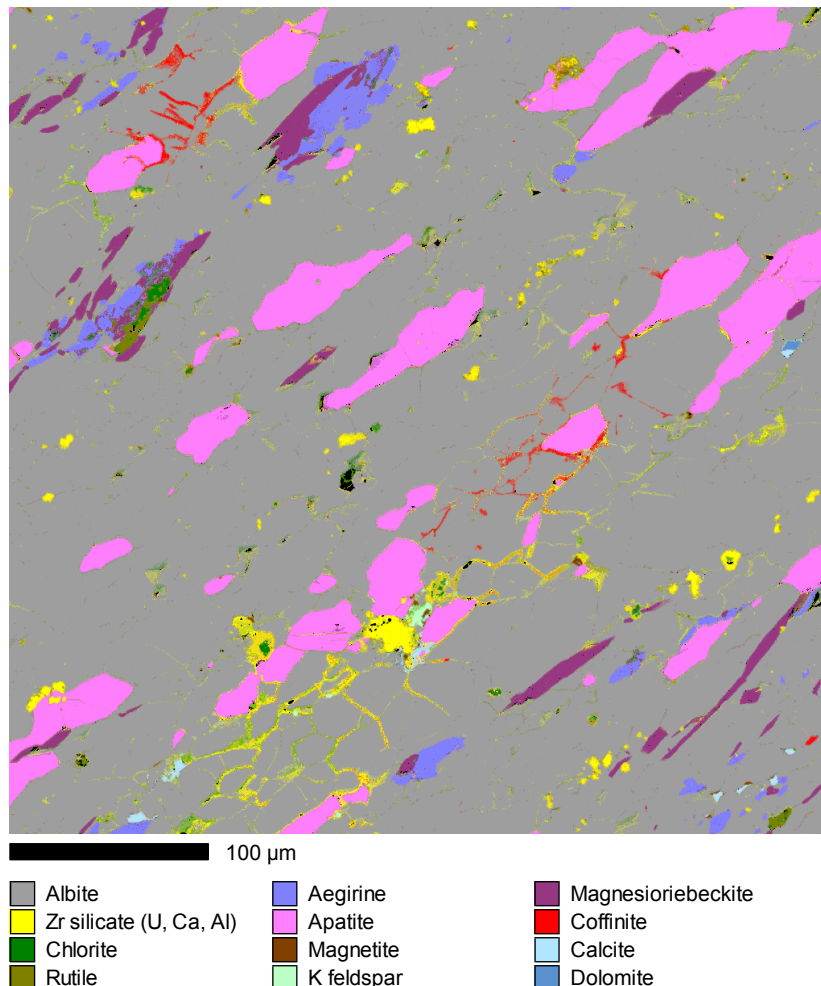


Figure 8. Phase patched map of sample from Valhalla drillhole VRD0126.

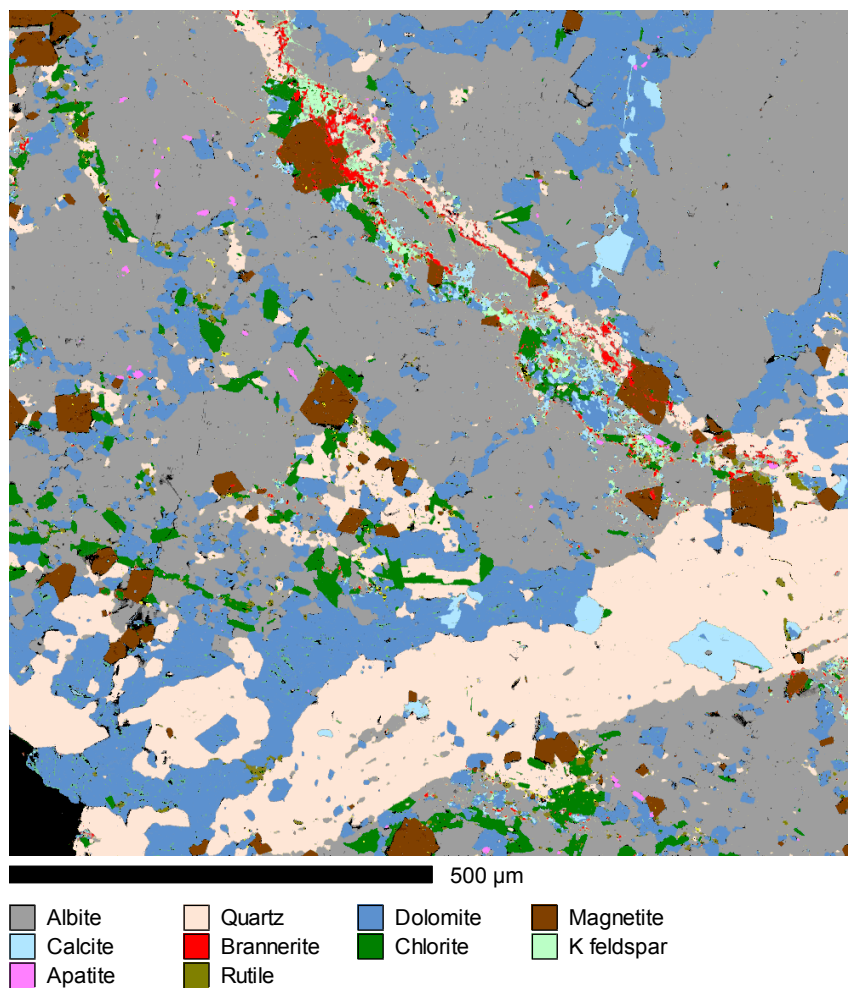


Figure 9. Phase patched map of sample from Valhalla drillhole VRD0205 163.1m region 3.

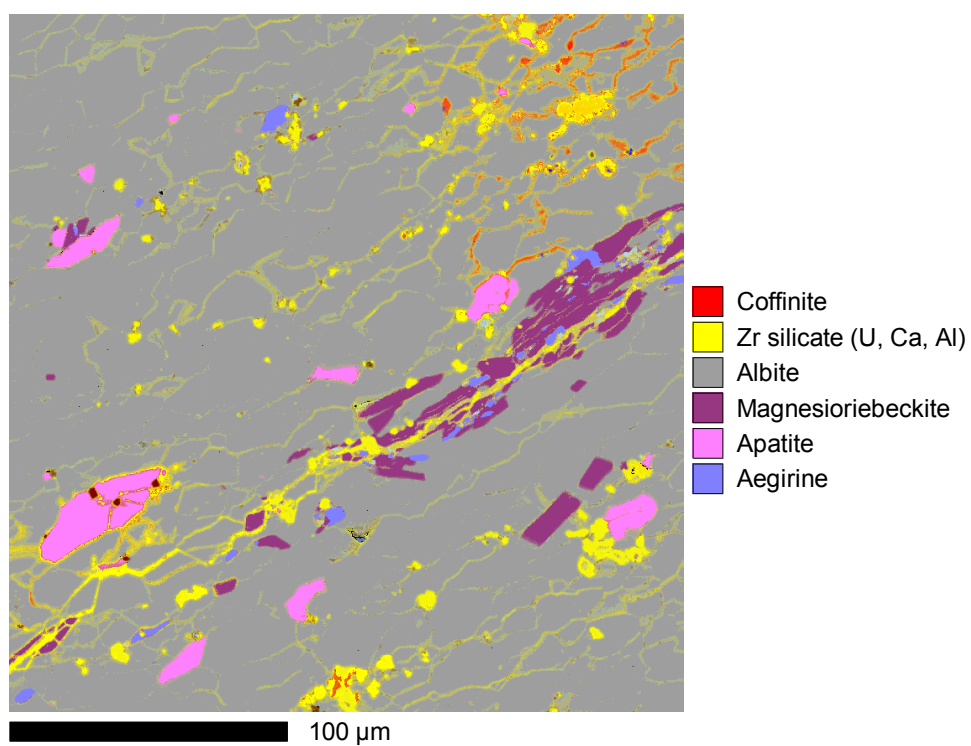
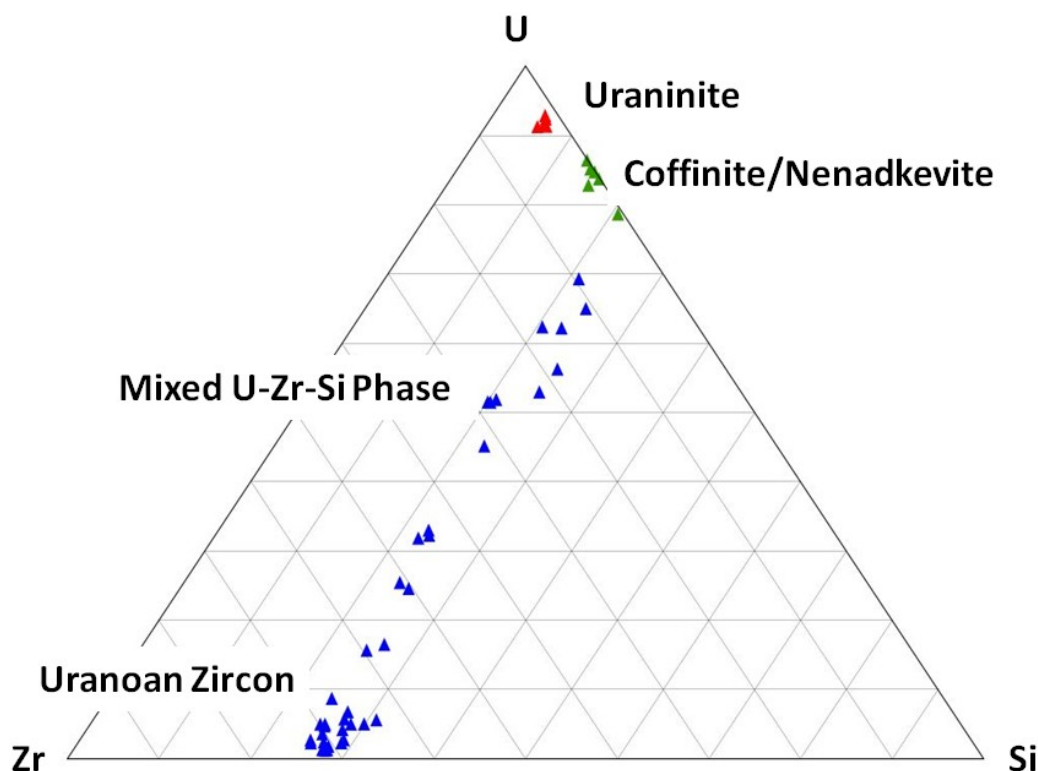


Figure 10. Ternary diagram illustrating range in composition of uranium minerals from Valhalla, Skäl and Bikini. “Uranoan zircon” refers to early subhedral inclusions in albite rather than later microveinlets along grain boundaries.



4.3. Skäl Mineralogy and Paragenesis

Fifteen samples from Skäl were quantified using QEMSCAN. Brannerite was found to be the most abundant uranium phase in all but one sample, where coffinite dominates. Uraninite is present in small amounts but the U-Zr phase was not detected at all. Skäl gangue is dominated by quartz and albite (55%) while chlorite and calcite account for a further 25% (Table 2). Only traces of amphibole have been detected and no pyroxene. Apatite is a ubiquitous hydrothermal phase (average 5%), reaching a maximum of 45%. Zircon and uraniferous zircon are much less abundant than at Valhalla (Table 2). Early alteration at Skäl differs appreciably from that at Valhalla, in that albite is less abundant whereas calcite, chlorite and quartz interact in complex textures that are hard to interpret.

Much of the uranium at Skäl occurs as irregular and discontinuous veinlets of brannerite, typically less than 100 μm in thickness, and typically associated with K-feldspar, biotite, ilmenite and rutile (Figures 11 and 12). The veinlet pictured in Figure 11 shows brannerite in an irregular veinlet of quartz with inclusions of ilmenite, biotite and rutile. Overall, Ti oxides are more abundant as veinlets than uranium minerals. The quartz vein is cut by discontinuous veinlets and patches of brannerite and K-feldspar. Calcite is a component of the veinlets in some cases but in others biotite-K-feldspar veins clearly cut and brecciate early calcite. In other samples brannerite was observed to occupy fractures in K-feldspar and to rim and envelope rutile and composite ilmenite/rutile grains.

Coffinite also occurs as veinlets, associated with biotite and chlorite and gradational to brannerite-rich portions. Several samples, however, also contain coffinite as rounded inclusions in albite. In many samples coffinite is intimately intergrown with brannerite.

Figure 11. Phase patched map of sample SRD0078B from Skal.

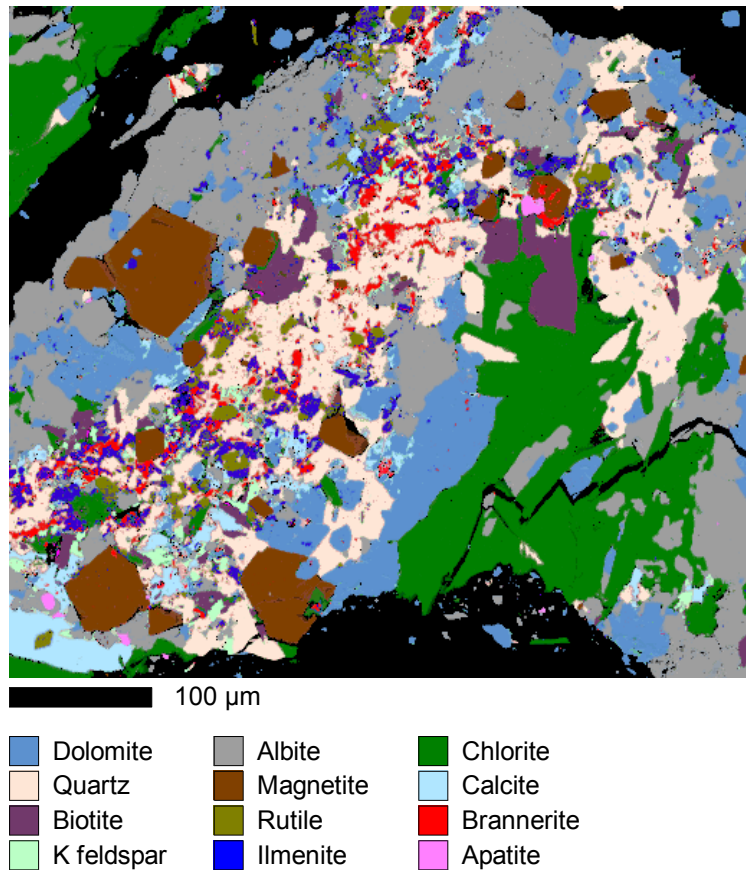
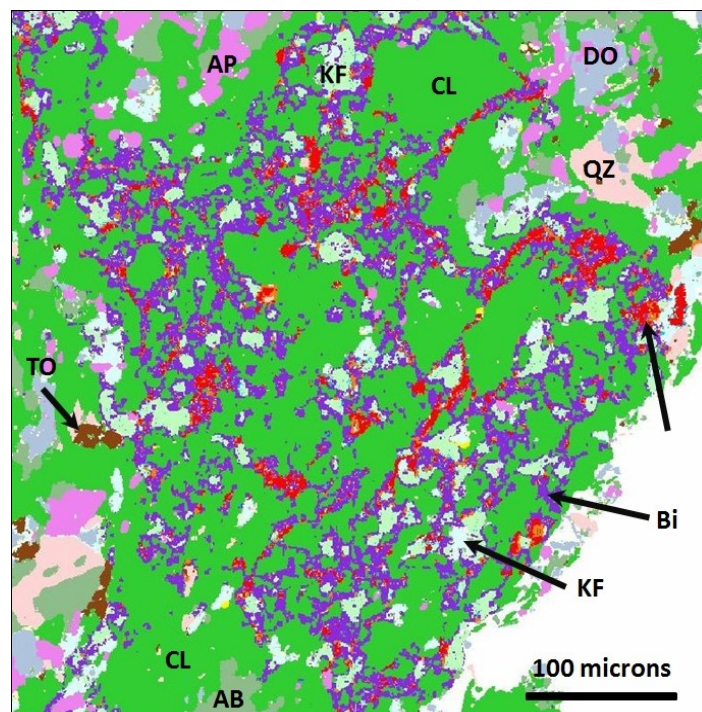


Figure 12. QEMSCAN image showing incipient breccia of chlorite-rich domain with network of biotite and K-feldspar veinlets with brannerite and Ti oxides. SD083 69.2 m. AB, albite; AP, apatite; BI, biotite; DO, ferroan dolomite; KF, K-feldspar; QZ, quartz; TO, Ti oxide. Brannerite is red and sulphide yellow.



4.4. Bikini Mineralogy and Paragenesis

Twelve samples from Bikini were quantified using QEMSCAN (Table 1). Bikini uranium mineralogy appears to be similar to Skal, in that brannerite is the most abundant phase. Brannerite is the dominant phase in all but one sample, where coffinite is dominant. Uraninite has not yet been detected at Bikini and nor has uraniferous zircon.

Bikini gangue phases are dominated by albite and quartz (60%). Amphibole and pyroxene are rare whereas carbonate, chlorite and white mica (collectively, 27%) are significantly more abundant than at Valhalla.

As at Skal, Bikini uranium occurs as irregular and discontinuous veinlets of brannerite associated with the potassic gangue minerals, K-Feldspar and biotite.

4.5. Other Deposits

Recent bulk geochemical analyses of samples from the Duke Batman deposit reveal overall similarity to Valhalla [21]. A key difference is generally higher K₂O content (average 0.93%) and much lower SiO₂ content (average 40.4%) of the mineralised samples. Mineralised Duke Batman samples show good correlation between uranium and HFSE, particularly Th (0.98), Y (0.81), Zr (0.62), Hf (0.59) and the REE except Nd (0.66–0.81). The HREE are relatively more abundant than the LREE. Other elements or oxides correlating with uranium are Sr (0.90), K₂O (0.78), Co (0.73), Zn (0.62), V (0.62) and Rb (0.60).

Quantitative mineralogical data for Anderson's Lode, Bambino, Father's Day, Neo, Queen's Gift, Slance, Thanksgiving and Watta are summarised in Figure 13. QEMSCAN was unable to resolve uranium mineralogy in some cases, due to the extreme fine grain size of the uranium phases. The Thanksgiving and Bambino deposits in particular proved problematic for uranium mineral identification. Nevertheless, we interpret these data to reflect the presence of two main ore types, predominantly brannerite, as at Anderson's Lode, Bikini, Father's Day, Queen's Gift, Skal and Slance, and predominantly uraninite and coffinite as at Valhalla, Watta and Neo.

Anderson's Lode has been the subject of a previous mineralogical investigation which revealed brannerite as inclusions in fluorapatite along with anatase [4]. Gold concentrations of up to 863ppb were recorded using bulk chemistry [4] but no discrete gold grains were observed using QEMSCAN. QEMSCAN did affirm the dominance of microvein brannerite and its spatial association with Ti oxide and titanite and biotite.

Relative masses of gangue minerals for the other deposits are shown in Table 3. The bulk of all the analysed samples comprise carbonate minerals, apatite, quartz and albite. The ratios of these minerals differ substantially. Father's Day, Neo and Honey pot samples are composed primarily of apatite and carbonate. The number of analysed samples for these deposits is low, however, and the degree to which these samples are representative of the whole is uncertain. Hydrothermal zircon was found in substantial masses in samples from Duke Batman (14.4%), Honey pot (7.98%) and Watta (4.77%).

Hydrothermal tourmaline is not a common phase but occurs with quartz in veins at Duke Batman [21] and is suggested to be synchronous with uranium at Anderson's Lode [4].

Figure 13. Proportions of uranium minerals in various deposits of the Mount Isa district, as determined by QEMSCAN. Note the major proportion of minerals that could not be reliably identified. There are two end-member mineralogies: uraninite-coffinite ore and brannerite ore. U-Zr minerals seem to be a feature of the Valhalla deposit, but host only a small portion of the uranium.

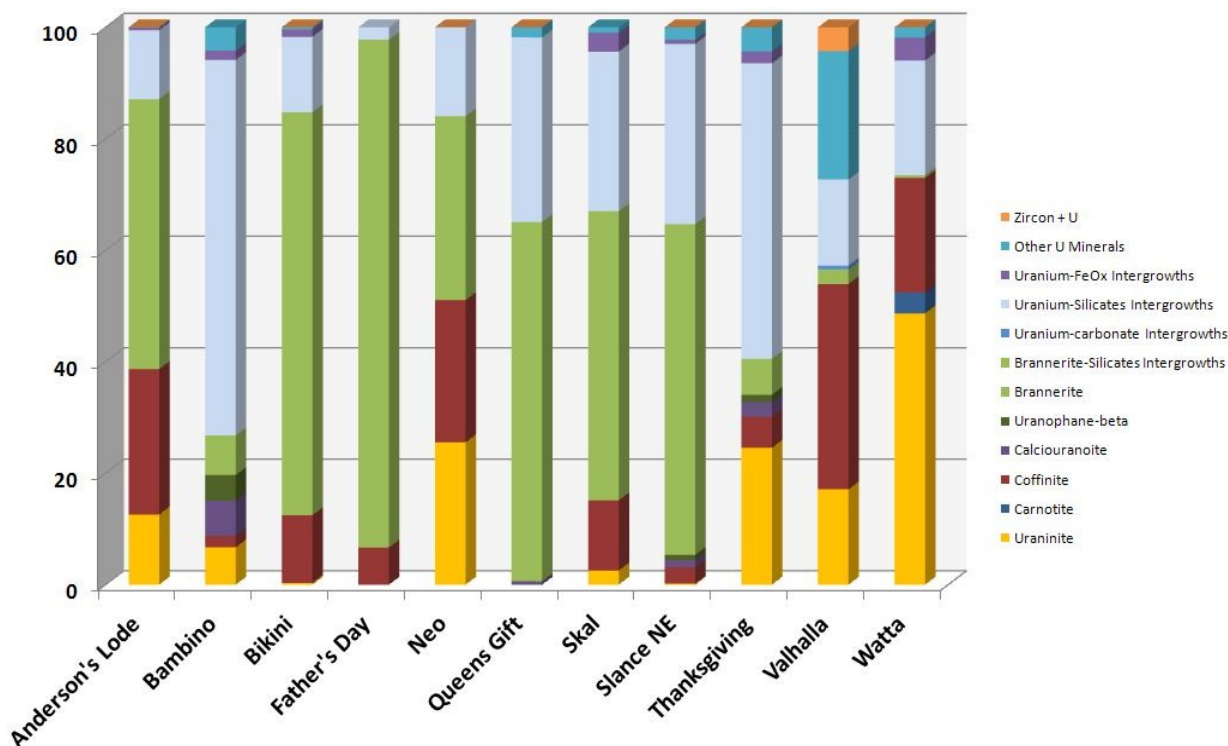


Table 3. Quantitative QEMSCAN modal analyses of gangue minerals from samples of nine uranium deposits from Mount Isa. Note that QEMSCAN did not detect aegirine in samples from Valhalla, although this mineral was detected using the hyperprobe.

Deposit	Sample #	U Minerals	Fe Oxides	Ti Oxides	Total Carbonate	Sulphides	Apatite	Quartz	Albite	K-feldspar	Zircon	Na-Pyroxene	Amphiboles	Micas	Chlorite
Anderson's Lode	9	2.5	3.4	1.2	11.3	0.1	18.7	18.0	13.9	bld	0.03	nd	2.4	14.0	10.3
Bikini	12	1.1	4.3	1.4	16.0	0.1	2.0	20.5	40.8	0.3	0.26	0.1	0.5	4.3	6.9
Duke Batman	2	0.2	4.6	1.3	25.3	0.2	6.1	19.4	20.5	bld	14.42	0.7	2.4	1.1	1.5
Father's Day	1	0.0	1.6	1.9	46.1	0.0	35.0	10.6	0.4	bld	bld	nd	1.0	1.5	0.0
Honeypot	2	0.1	0.5	1.2	11.8	0.2	37.9	14.9	5.1	bld	7.98	0.5	2.9	1.4	6.1
Neo	1	0.0	0.0	0.3	4.4	0.0	52.5	8.1	20.5	bld	0.02	nd	2.6	6.9	2.9
Skal	15	0.7	3.4	2.4	15.0	1.0	5.1	29.9	24.8	0.3	0.24	0.1	2.1	3.5	10.4
Valhalla	19	1.6	3.6	4.3	8.9	1.3	7.8	6.0	41.4	bld	5.58	nd	13.4	nd	4.1
Watta	4	0.5	5.1	1.9	8.2	0.1	9.0	20.5	26.4	bld	4.77	0.1	1.1	15.1	3.9
Average	65	0.7	2.9	1.8	16.3	0.3	19.4	16.4	21.5	0.3	4.16	0.3	3.2	6.0	5.1

5. Discussion

5.1. Paragenesis and Timing

Formation of the albite, magnetite, zircon and apatite assemblage at Mount Isa can be dated at pre- to syn-D₂ because of folding and transposition by the S₂ foliation and lineation that is defined principally by riebeckite [18–20]. The fact that the albitite bodies are exclusively found in D₂ high strain zones is a compelling argument for overall D₂ timing. The presence of laminated (mylonitic) textures, strong foliation and transposed fold limbs suggests that albitisation is associated with intense ductile deformation localised in north-south trending shear zones.

This study has shown that a substantial portion of the uranium occurs as microveinlets, generally less than 100 µm in thickness. Such microveinlets typically contain either near monomineralic coffinite (and/or nenadkevite) or an assemblage of brannerite, ilmenite, rutile (or anatase), K-feldspar and biotite. This potassic assemblage contrasts with the sodic host albitite and is indicative of brittle rather than ductile deformation. The abundance of potassic phases is not sufficient in most cases to result in appreciable bulk-rock enrichment of K. The exception is Duke Batman, which has notably higher potassium contents relative to other deposits. Uraninite in nearly all cases comprises below 20% of total uranium minerals, and in several deposits has not been detected at all. Evidence from Valhalla suggests that uraninite occupies relatively late veinlets that postdate coffinite and brannerite [3].

Carbonate appears to be both pre- and post-uranium. Dolomite, ankerite and calcite associated with albitite are cut by uranium-bearing veins but calcite, chlorite, epidote and sulphide veining is also demonstrably late [3] and clearly a brittle phenomenon. This accords with observations of regional carbonate-iron oxide veins cutting the S₂ fabric [6]. Chlorite is also associated with NW-SE trending faults thought to be of D₃ age [14]. The published ²⁰⁷Pb/²⁰⁶Pb Valhalla brannerite age of 1543 ± 15 Ma [3] is somewhat younger than the peak metamorphic age of 1590 Ma. This is consistent with our conclusion that uranium was emplaced after peak deformation. An implication of this is that the host-rocks are likely to have been undergoing cooling from the metamorphic peak during uranium deposition. Valhalla uraninite has been dated at 1220 ± 12 Ma using the ^{207/206}Pb technique [3] but is possibly afflicted by loss of radiogenic daughters.

5.2. Comparison with Other Albitite-Type Deposits

There are many similarities and few differences between the albitite-type deposits of Mount Isa and other albitite-type deposits such as those of the Kirovograd district of the Ukraine, Manibay in Kazakhstan and Kurupung in Guyana. Whereas the main ore hosts at Mount Isa are metabasalt and metasiltstone, ore at Kurupung is hosted within a monzonite intrusion, while the Kirovograd deposits are hosted within a wide variety of granitoids and metamorphic rocks, including some unusually iron-rich lithologies [1,30–33].

A common characteristic of the deposits is the association of uranium with sodic alteration manifested as albitite and occurring within ductile (mylonitic) deformation zones [1,30–33]. Early albitites typically contain the sodic phases riebeckite and aegirine, particularly in the deeper and interior parts of the orebodies [33,34]. Vertical zonation of post-albitite phases has been observed in some Kirovograd deposits, where potassic assemblages (containing phlogopite) tend occur at depth,

while chlorite-carbonate and hematite assemblages dominate nearer the surface [33]. While we have not observed such zonation at Mount Isa, there appear to be substantial variations in gangue mineralogy between individual deposits. Valhalla has by far the highest volume of amphibole and pyroxene, suggesting that it formed from hydrothermal fluids of different composition to those that formed Skal and Bikini or that Valhalla formed at higher temperature.

Evolution from ductile deformation of albitite to brittle-control with uranium deposition has been previously described in the Kirovograd deposits where uranium mineralisation is best developed in areas subject to “post-albitite cataclasis” [33]. This mirrors our observations at Mount Isa and can be rationalised as due to declining temperature as mineralisation proceeded. The transition from sodic to potassic alteration and gangue can also be explained as due to declining temperature.

The uranium minerals and mineral assemblages at Mount Isa described herein are similar to those documented in other albitite-type deposits, where uraninite, coffinite, brannerite, nenadkevite and uranoan or uraniferous zircon are commonly described [2,3,29,31–34].

The variability of host rock bulk chemical composition and mineralogy (between deposits) suggests that a particular fluid-rock reaction is not the critical process by which uranium precipitates, and indeed that wall-rock reaction may not be important. Alternatively it could be argued that most rock-types have the capacity to buffer fluid composition and to precipitate uranium in whatever form it is introduced. The possibility of reduction of the ore-forming fluid by (for example) magnetite has been explored for some of the Kirovograd deposits, but lack of evidence for oxidation of Fe^{2+} has suggested this is not a viable precipitation mechanism [35]. Conversely, the consistent mineralogy of the early albitites in a large number of deposits and irrespective of host-rock lithology is indicative of control of the bulk system composition by the hydrothermal fluid or fluids, rather than by the host-rocks. Thus cooling, for example as hydrothermal fluids move from a hot source to cooler surrounds, is a potential depositional mechanism. Another possible mechanism could be pressure changes and/or exsolution of a gas phase from a previously homogeneous fluid during brittle fracture of the albitite host rocks and formation of microveins. The processes of uranium deposition remain uncertain, however, and deserve further research.

5.3. Hydrothermal U-Zr Phase

Uranium-rich zircons and “zircon-like” phases appear to be a characteristic feature of albitite-type uranium deposits. Uranium occurs both within the zircon crystal lattice and as fracture-filling minerals [30,31]. The Kurupung deposit contains substantial volumes of hydrothermal uranoan “zircon” deposited in vugs with albite and as veins up to 1 cm wide [30]. Amorphous zircon has been reported at the Manibay uranium mine, Kazakhstan as veins in P-Zr-U ore, and containing up to 9.14% UO_2 [33].

Our study shows that Zr-bearing phases at Mount Isa range in composition from zircon *sensu stricto*, containing minor amounts of uranium (previously referred to as “uranoan zircon” [2,3]), to a U-Zr silicate in which the amount of uranium exceeds the amount of zirconium (Figure 10) and which cannot, therefore, be zircon. This unnamed U-Zr silicate shows complete solid solution with a uranium silicate, possibly nenadkevite (Figure 10).

There is some evidence of Zr depletion at the margin of early zircon (*sensu stricto*) and one plausible explanation for the unnamed U-Zr phase at Valhalla is that it represents the reaction of a late-stage hydrothermal fluid with a rock previously enriched in hydrothermal Zr. Nevertheless, the conclusion that the overall mineralising process introduced large volumes of Zr seems inescapable.

Large volumes of hydrothermal Zr-rich minerals occur in association with certain alkaline intrusive complexes and carbonatites [36–38]. Theoretical and experimental considerations suggest low Zr solubility in aqueous fluids as $Zr(OH)_4$ [39]. However, if the system contains high levels of fluorine (~0.1 m aqueous F) Zr concentrations in excess of 10 ppm can be anticipated at <200 °C [40]. Fluorine also forms stable aqueous complexes with uranium, and complexing of uranium (and other HFSE) by magmatic fluorine has been proposed to explain the vast uranium and REE endowment of the super-giant Olympic Dam copper-uranium deposit [41].

5.4. An Evaluation of Published Genetic Models

Previous discussions of the genesis of Mount Isa's albitite-type uranium deposits have appealed to a range of magmatic and basinal processes [3–6,9]. Stable isotopic evidence has been used to argue for the participation of basinal fluids, although it was acknowledged that the data did not rule out a magmatic fluid source [3]. A major objection to a basin model is the absence of a sedimentary basin that might supply basinal fluids at the inferred time of ore formation. By 1590 Ma, any suitable sedimentary rocks at Mount Isa would have experienced at least 100 Ma of diagenesis and compaction and would have been undergoing dehydration reactions during greenschist to amphibolites facies regional metamorphism [13,12]. We suggest therefore that the probability that the Mount Isa district uranium deposits were related to basin evolution is extremely small.

Metamorphic dehydration of meta-sediments and meta-volcanic rocks could have provided an ore-forming fluid, consistent with textural evidence placing albitite formation at the peak of D₂ regional deformation. The unusual bulk composition of the ores, notably enrichment in many HFSE, P and F (in apatite and riebeckite) is inconsistent with such an origin and indeed with a basinal source.

We suggest that the mineralogical and bulk chemical data are best interpreted in terms of a distal magmatic origin for the uranium and HFSE and that fluorine complexing of uranium (either in gaseous or aqueous form) was responsible for uranium transport. Indeed, published stable isotope data are consistent with a magmatic source for ore-forming fluids [3].

It is tempting to associate the deposits with the anomalously radioactive Kitty Plains microgranite, however, this has been shown to have been emplaced approximately 80 Ma prior to Valhalla [9]. A plausible alternative is the abundant pegmatites and quartz-tourmaline veins, and published radiometric ages and structural relationships are consistent with this interpretation [11,15]. Thus, we propose that uranium introduction into the albitites is genetically related to a magmatic event manifested by widespread intrusion of relatively small pegmatite dykes and veins.

6. Conclusions

Albitite-type uranium deposits of the Mount Isa district are comparable in many respects to other albitite-type uranium deposits, differing mainly in the fact that their host rocks are metabasalt and metasilstone. Mineralised albitites occur in transgressive D₂ ductile deformation zones and albitisation

probably overlapped peak D₂ deformation in time. Uranium postdates the early sodic alteration and is associated with microfracturing of the albitite. Vein-controlled uranium occurs as brannerite, coffinite (and/or nenadkevite), uraninite and an unidentified U-Zr silicate and is associated paragenetically with potassic phases such as K-feldspar and biotite as well as a TiO₂ polymorph (probably rutile), titanite and ilmenite. The association of U and HFSE argues for simultaneous transport in a F-rich hydrothermal fluid, and against transport in basinal brines or the products of metamorphic devolatilisation.

We propose that uranium mineralisation is genetically related to the intrusion of tourmaline and beryl-bearing pegmatites and quartz-tourmaline veins.

Acknowledgements

We thank Paladin Energy for permission to publish this paper. We acknowledge the significant contribution to unraveling the complex geology of the deposits by many unsung geologists including Daniel Jordan, Stuart Kerr, Mike Lee, Matt Porter, Andreas Stiehler, Jimmy Thom, Wendy Thomas and Cornelius “Corndog” Werth. Reviews by Nick Oliver, Paul Polito and an anonymous reviewer helped improve an early version of this manuscript.

Conflict of Interest

The authors declare no conflict of interest.

References

1. Wilde, A.R. Towards a model for albitite-type uranium. *Minerals* **2013**, *3*, 36–48.
2. Goldney, L.H.; Canning, R.G.; Gooden, J.E.A. *Extraction Investigations with Some Australian Uranium Ores*; AAEC Symposium on Uranium Processing; Australian Atomic Energy Commission: Adelaide, Australia, 1972; pp. 1–18.
3. Polito, P.; Kyser, K.; Stanley, C. The Proterozoic, albitite-hosted, Valhalla uranium deposit, Queensland, Australia: A description of the alteration assemblage associated with uranium mineralisation in diamond drill hole V39. *Miner. Depos.* **2007**, *44*, 11–40.
4. Gregory, M.; Wilde, A.; Jones, P. Uranium deposits of the Mount Isa region and their relationship to deformation metamorphism and copper deposition. *Econ. Geol.* **2005**, *100*, 537–546.
5. Wyborn, L. The Petrology and Geochemistry of Alteration Assemblages in the Eastern Creek Volcanics, as a Guide to Copper and Uranium Mobility Associated with Regional Metamorphism and Deformation, Mt Isa, Queensland. In *Geochemistry and Mineralization of Proterozoic Volcanic Suites*; GS Special Publication No. 33; Pharaoh, T.C., Beckinsale, R.D., Rickard, D., Eds.; Institute of Mining and Metallurgy: London, UK, 1987; pp. 425–434.
6. Bain, J.H.C.; Heinrich, C.A.; Henderson, G.A.M. Stratigraphy, Structure and Metasomatism of the Haslingdon Group, East Moondarra Area, Mt Isa: A Deformed and Mineralised Proterozoic Multistage Rift-sag Sequence. In *Detailed Studies of the Mount Isa Inlier*; Australian Geological Survey Organisation Bulletin 243; Stewart, A.J., Blake, D.H., Eds.; Australian Geological Survey Organisation: Canberra, Australia, 1992; pp. 125–136.

7. Perkins, C.; Heinrich, C.; Wyborn, L. $^{40}\text{Ar}/^{39}\text{Ar}$ geochronology of copper mineralization and regional alteration, Mount Isa, Australia. *Econ. Geol.* **1999**, *94*, 23–36.
8. Page, R. Chronology of magmatism, skarn formation, and uranium mineralization, Mary Kathleen, Queensland, Australia. *Econ. Geol.* **1983**, *78*, 838–853.
9. McGloin, M. U-Pb Shrimp geochronology of the Sybella microgranite: Is there a link to U-Ree prospects at Mount Isa? *AIG News* **2012**, *110*, 29–30.
10. Gregory, M.J.; Schaefer, B.F.; Keays, R.R.; Wilde, A.R. Rhenium-Osmium systematics of the Mount Isa copper orebody and the Eastern Creek volcanics, Queensland: Implications for ore genesis. *Miner. Depos.* **2008**, *43*, 553–573.
11. Connors, K.A.; Page, R.W. Relationship between magmatism, metamorphism and deformation in the western Mount Isa Inlier, Australia. *Precambrian Res.* **1995**, *71*, 131–153.
12. Huang, W.; Rubenach, M. Structural controls on syntectonic metasomatic tremolite and tremolite-plagioclase pods in the Molanite Valley, Mt Isa, Australia. *J. Struct. Geol.* **1995**, *17*, 83–94.
13. Abu Sharib, A.S.; Sanislav, I.V. Polymetamorphism accompanied switching in horizontal shortening during Isan Orogeny: Example from the Eastern Fold Belt, Mount Isa Inlier, Australia. *Tectonophysics* **2012**, *587*, 146–167.
14. Wilde, A.R. Mount Isa copper orebodies: Improving predictive discovery. *Aust. J. Earth Sci.* **2011**, *58*, 937–951.
15. Duncan, R.; Wilde, A.R.; Bassano, K.; Maas, R. Geochronological constraints on tourmaline formation in the Western Fold Belt of the Mount Isa Inlier, Australia: Evidence for large-scale metamorphism at 1.57 Ga? *Precambrian Res.* **2006**, *146*, 120–137.
16. Hannan, K.; Golding, S.D.; Herbert, H.K.; Krouse, H.R. Contrasting alteration assemblages in metabasites from Mount Isa, Queensland: Implications for copper ore genesis. *Econ. Geol.* **1993**, *88*, 1135–1175.
17. Heinrich, C.A.; Bain, J.H.C.; Mernagh, T.P.; Wyborn, L.A.I.; Andrew, A.S.; Waring, C.L. Fluid and mass transfer during metabasalt alteration and copper mineralization. *Econ. Geol.* **1995**, *90*, 705–730.
18. Oliver, N.H.S. *Appraisal of Structural Geology and Controls on Mineralization in the Valhalla Region*, 2010; p. 30; Unpublished Report to Summit Resources, Holcombe Coughlin Oliver Consultants.
19. Oliver, N.H.S. *Appraisal of Structural Geology and Controls on Mineralization in the Valhalla Region (Part 2)*, 2010; p. 30; Unpublished Report to Summit Resources, Holcombe Coughlin Oliver Consultants.
20. Oliver, N.H.S. *Prospectivity, Structure and Geochemistry in the Valhalla District*, 2010; p. 19; Unpublished Report to Summit Resources, Holcombe Coughlin Oliver Consultants.
21. Werth, C. Petrography and Geochemistry of the Duke Batman Uranium Deposit in Northwestern Queensland, Australia. Master's Thesis, RWTH Aachen University, Aachen, Germany, 10 September 2012.
22. Anonymous. *QEMSCAN Analysis Valhalla Uranium Thin Sections*, 2009; Unpublished AMDEL Report N3437QS09.
23. De Nooy, D.; Hodgson, W. *Mineralogical Investigation of Twenty Polished Thin Sections Using QEMSCAN and SEM-EDS Methods*, 2010; Job NO: S0591; SGS Report to Summit Resources.

24. Hodgson, W.; de Nooy, D.; Lonsdale, G. *Mineralogical Investigation of Ten Polished Thin Sections Using QEMSCAN and SEM-EDS Methods*, 2009; SGS Report to Summit Resources.
25. Armstrong, J.T. CITZAF: A package of correction programs for the quantitative electron microbeam X-ray-analysis of thick polished materials, thin films, and particles. *Microbeam Anal.* **1995**, *4*, 177–200.
26. Harrowfield, I.R.; MacRae, C.M.; Wilson, N.C. Chemical Imaging in Electron Microprobes. In Proceedings of the 27th Microbeam Analysis Society Annual MAS Meeting, New York, NY, USA, 1993; pp. 547–548.
27. Wood, D.A.; Joron, J.L.; Treuil, M.; Norry, M.; Tarney, J. Elemental and Sr isotope variations in Basic Lavas from Iceland and the surrounding ocean floor. *Contrib. Miner. Petrol.* **1979**, *70*, 319–339.
28. Lumpkin, G.R.; Leung, S.H.F.; Colella, M. Position, Geochemical Alteration, and Alpha-Decay Damage Effects of Natural Brannerite. In Proceedings of 23th International Symposium on Scientific Basis for Nuclear Waste Management, Boston, MA, USA, 29 November–2 December 1999; pp. 359–365.
29. Polikarpova, V.A. Nenadkevite—A new silicate of uranium. *J. Nucl. Energy* **1957**, *4*, 262–265.
30. Alexandre, P. Mineralogy and geochemistry of the sodium metasomatism-related uranium occurrence of Aricheng South, Guyana. *Miner. Depos.* **2009**, *45*, 351–367.
31. Cinelu, S.; Cuney, M. Sodic metasomatism and U–Zr mineralization: A model based on the Kurupung batholith (Guyana). *Goldschm. Conf. Abstr.* **2006**, *70*, A103.
32. Omel'yanenko, B.I.; Mineyeva, I.G. Pre- and Syn-Ore vertical zonation in Precambrian uraniferous sodic metasomatites. *Int. Geol. Rev.* **1982**, *24*, 422–430.
33. Helean, K.B.; Burakov, B.E.; Anderson, E.B.; Strykanova, E.E.; Ushakov, S.V.; Ewing, R.C. Mineralogical and microtextural characterization of “gel-zircon” from the Manibay uranium mine, Kazakhstan. *Mat. Res. Soc. Symp. Proc.* **1997**, *465*, 1219–1226.
34. Zhukova, V.Y. Mineralogy and Primary Zoning of Hydrothermal Metasomatic Uranium Deposits in Precambrian Iron Formations. In *Albitized Uranium Deposits: Six Articles Translated from Russian Literature*; Report GJBX-193; Avrashov, A., Abou-Zied, S., Kerns, G., Eds.; U.S. Department of Energy: Washington, DC, USA, 1980; pp. 91–112.
35. Cuney, M.; Emetz, A.; Mercadier, J.; Mykchaylov, V.; Shunko, V.; Yuslenko, A. Uranium deposits associated with Na-metasomatism from central Ukraine: A review of some of the major deposits and genetic constraints. *Ore Geol. Rev.* **2013**, *44*, 82–106.
36. Sheard, E.; Williams-Jones, A.; Heiligmann, M.; Pederson, C.; Trueman, D. Controls on the concentration of zirconium, niobium and the rare earth elements in the Thor Lake rare metal deposit, Northwest Territories, Canada. *Econ. Geol.* **2012**, *107*, 81–104.
37. Guimaraes, D. The Zr Ore deposits of the Pocos de Caldas Plateau, Brazil and Zr chemistry. *Bol. Inst. Tecn. Ind. Minas Gerais* **1948**, *6*, 1–40.
38. Kuschke, O.; Tonking, M. Geology and mining operations at Palabora Mining Company Ltd, Phalaborwa, NE Transvaal. *J. South Afr. Inst. Min. Met.* **1971**, *72*, 12–22.
39. Aja, S.U.; Wood, S.A.; Williams-Jones, A.E. The aqueous geochemistry of Zr and the solubility of some Zr-bearing minerals. *Appl. Geochem.* **1995**, *10*, 603–620.

40. Migdisov, A. The solubility of Zr in F-bearing hydrothermal solutions. *Geochim. Cosmochim. Acta* **2009**, *73*, A879.
41. Chambefort, I.; Kamenetsky, V.; McPhie, J.; Bath, A.; Agangi, A.; Allen, S.R.; Ehrig, K.; Green, N. The Olympic Dam Cu-Au-U Deposit, South Australia: Was Fluorine a Key in Forming this Giant? In Proceedings of the Tenth Biennial SGA Meeting, Townsville, Australia, 2009; pp. 207–209.

© 2013 by the authors; licensee MDPI, Basel, Switzerland. This article is an open access article distributed under the terms and conditions of the Creative Commons Attribution license (<http://creativecommons.org/licenses/by/3.0/>).